# Analytic Field Propagation TFSF Boundary for FDTD Problems Involving Planar Interfaces: PECs, TE, and TM

John B. Schneider, *Member, IEEE*, and Kakhkhor Abdijalilov

***Abstract*—A total-field scattered-field (TFSF) boundary can be used to introduce incident plane waves into finite-difference time-domain (FDTD) simulations. For fields which are traveling obliquely to the grid axes, there is no simple way to account fully for the effects of the inherent numerical artifacts associated with plane-wave propagation in the FDTD grid. Failure to account for these artifacts causes erroneous fields to leak across the TFSF boundary. Recent publications have proposed ways to use the dispersion relation to describe precisely plane-wave propagation in the FDTD grid thus permitting the realization of a nearly perfect TFSF boundary. However, these publications did not cover certain implementations details (such as the type of Fourier transform which is needed) or their scope was so broad as to mask the relative simplicity with which the approach can be applied to problems involving planar interfaces. This work considers the Fourier transforms needed in order for the implementation to be exact. Reflection and transmission coefficients for a planar interface are derived. Implementation for planar perfect electric conductors is also presented.**

***Index Terms*—Finite-difference time-domain (FDTD) methods.**

## I. Introduction

THE total-field scattered-field (TFSF) formulation is a method for introducing energy into a finite-difference time-domain (FDTD) simulation. It defines a boundary, identified as the TFSF boundary, which divides the computational domain into two regions: a total-field (TF) region which contains both the incident field and any scattered field, and a scattered-field (SF) region which contains only scattered fields. Scatterers are confined to exist within the TF region. Throughout the grid the fields must have self-consistent update equations meaning that nodes in the TF region must depend on the total field at neighboring nodes while nodes in the SF region must depend on the scattered field at neighboring nodes. However, nodes which are tangential to the TFSF boundary will have at least one neighboring node in the region different from their own. Rectification of this inconsistency is what drives the TFSF method.

Given knowledge of the incident field which should exist at nodes tangential to the TFSF boundary, one does the following. For the update of a node which is in the TF region and depends on a neighboring node in the SF region, the incident field is added to that neighboring node. Conversely, for the update of a node which is in the SF region and depends on a neighboring node in TF region, the incident field is subtracted from that neighboring node. In this way the TFSF boundary acts as a Huygens surface and was originally described as such by Merewether *et al.* [1].

In order to implement the TFSF method, one must know the incident field at every time-step at all the tangential nodes adjacent to the boundary. Historically the TFSF method has been used to introduce plane waves into the grid, but in theory any incident field could be realized. In this work we restrict ourselves to plane waves. In the continuous world, the analytic description of pulsed plane-wave propagation is relatively trivial. Unfortunately, because of the inherent difference between the way in which waves propagate in the FDTD grid and the way in which they propagate in the continuous world, one should not simply use the continuous-world expression for the incident plane wave. If one were to do that, the mismatch between the analytic description of the incident field and how the incident field actually propagates within the grid causes fields to leak across the TFSF boundary (in the absence of a scatterer, no fields should be present in the SF region). Fortunately there is a relatively simple fix to this problem for grid-aligned propagation.

An auxiliary one-dimensional (1-D) FDTD simulation can be implemented to model the propagation of the incident plane wave. If the propagation direction of the incident field in a higher-dimensional grid is aligned with one of the grid axes, the auxiliary 1-D grid can be used to describe exactly the incident field at all nodes adjacent to the TFSF boundary. There is no leakage. A detailed discussion of the implementation can be found in [2].

When the incident field propagates obliquely, a one-dimensional auxiliary grid can still be used to describe, at least approximately, the incident field. However, using these fields in the higher-dimensional simulation has inherent errors. First, interpolation must be used to find the fields at points on the 1-D grid corresponding to the projected locations of nodes in the higher-dimensional grid. Implementation details for oblique propagation can also be found in [2]. Second, the dispersion which the fields experience in the 1-D grid does not correspond to the dispersion experienced in the higher-dimensional grid. To help rectify this, Guiffaut and Mahdjoubi [3] proposed a technique which modified the Courant number in the auxiliary grid so that the dispersion nearly matched that of the higher-dimensional grid (see also [2, Sec. 5.9.1]). Nevertheless, there are still differences between propagation in the two grids and the need

Manuscript received November 11, 2005; revised March 30, 2006. This work was supported by the Office of Naval Research Code 321OA.

The authors are with the School of Electrical Engineering and Computer Science, Washington State University, Pullman, WA 99164-2752 USA (e-mail: schneidj@eecs.wsu.edu).

Digital Object Identifier 10.1109/TAP.2006.880757

for interpolation, which inherently introduces errors, still exists. Third, the orientation of vector fields is not the same in the FDTD grid as it is in the continuous world. This fact is discussed in [4], [5] and had been considered previously in [6], [7]. The orientation is dependent on frequency and hence a simple scalar cannot be used to project field components from a 1-D grid to a higher-dimensional grid.

Despite these inherent errors in the 1-D auxiliary grid approach, the technique is relatively simple to implement, is efficient, and can be sufficiently accurate for many applications. Further improvements can be made to the technique such as proposed in [8], [9] where better interpolation methods were proposed. Another TFSF approach which is based on multiple auxiliary one-dimensional grids but permits layered and dispersive media was present by Winton *et al.* [10]. Previously the implementation of a TFSF boundary for layered media had been considered in [11], but that work did not account for the differences between the continuous world and the FDTD grid. The idea of using an auxiliary grid to model the incident field has also been extended to a multi-dimensional auxiliary grid. This provides a means to realize a TFSF boundary which does not leak. The interested reader is referred to [12], [13] which also describes the use of non-plane-wave sources.

Instead of employing an auxiliary grid, two recent papers proposed a technique where the incident field is obtained analytically by way of the FDTD dispersion relation [4], [5]. To distinguish this approach from that which relies upon auxiliary grids, we label this approach the analytic field propagation (AFP) TFSF technique. Moss *et al.* considered the situation of a field incident on layered uniaxial anisotropic media and hence had to account for the reflection and transmission coefficients of the layers [4]. Schneider restricted consideration to propagation in a homogeneous space [5].

Because of the complexity of the media being considered by Moss *et al.*, the equations given in their work masked the simplicity which pertains for problems involving isotropic media and problems involving a perfect electrically conducting (PEC) plane. In this work we examine these problems in some detail and obtain equations which are significantly simpler than those presented for anisotropic media. As described both by Moss *et al.* [4] and Schneider [5], the AFP TFSF method requires Fourier transforms to obtain the incident field. However, neither of those papers provided details of the type of transform actually need. In fact, an exact implementation requires not a discrete Fourier transform but rather a discrete-time Fourier transform (which involves a continuous integral). As will be discussed, this transform can be approximated by a discrete transform, but one should be aware of the inherent approximation.

This paper begins by providing an overview of the AFP TFSF technique as well as discussing the issues concerning the Fourier transform. We then consider problems involving a PEC plane or a planar dielectric interface. Both TE and TM polarization are considered.

## II. The AFP TFSF Method

Any implementation of a TFSF boundary requires knowledge of the incident field at nodes adjacent to the boundary for every time-step of the simulation. Conceptually, the AFP version of the TFSF method is quite simple in that it parallels the usual description of propagation in the continuous world.

In the continuous world, the spatial dependence of a harmonic plane wave is given by $\exp(-j\mathbf{k}\cdot\mathbf{r})$ where $\mathbf{k}$ is the wave vector and $\mathbf{r}$ is the position vector ($\exp(j\omega t)$ temporal dependence is understood). For a pulsed plane wave each spectral component can be weighted by the appropriate amount to give the frequency-domain representation. So, for example, if a field component were found at the origin to be given in the time-domain by $f(t)$, its frequency-domain representation would be $F(\omega)=\mathcal{F}[f(t)]$ where $\mathcal{F}[]$ is the Fourier transform. The field at an arbitrary point $\mathbf{r}$ merely has to account for the displacement from the origin. Thus in the frequency domain the field is given by $F(\mathbf{r},\omega)=F(\omega)\exp(-j\mathbf{k}\cdot\mathbf{r})$. The time-domain signal at $\mathbf{r}$ is the inverse transform of this, i.e.

$$f(\mathbf{r},t)=\frac{1}{2\pi}\int_{-\infty}^{\infty}F(\omega)e^{-j\mathbf{k}\cdot\mathbf{r}}e^{j\omega t}d\omega. \tag{1}$$

Assuming lossless media, in the continuous world the magnitude of the wave vector is given by $\omega/c$ where $c$ is the speed of light. Thus it is straightforward to evaluate—the complex exponential involving space merely represents a shift operation.

In the discretized world of the FDTD method, one can follow steps which parallel those in the continuous world. However, finding the field at an arbitrary point is complicated by the fact that the wave vector in the grid is governed by the FDTD dispersion relation which does not, in general, have a closed-form solution. Nevertheless, it is relatively easy to solve for the wave vector and to perform the necessary transforms to calculate the incident field wherever it is needed.

Since the input signal is not periodic, one cannot use a discrete Fourier transform (which inherently assumes a periodic signal). Instead, for a transient signal, one must use the discrete-time Fourier transform [14]. The inverse and forward transforms of the discrete signal $f(q\Delta)=f[q]$ are given by

$$f[q]=\frac{1}{2\pi}\int_{0}^{2\pi}F(\omega')e^{j\omega' q}d\omega' \tag{2}$$

$$F(\omega')=\sum_{q=-\infty}^{\infty}f[q]e^{-j\omega' q}. \tag{3}$$

Note that, despite this transform pertaining to a discretized world, the frequency $\omega'$ is a continuous variable. In FDTD, any "source function" $f[q]$ can be assumed to start at $q=0$ and be limited to a maximum of $N_s$ time steps (i.e., the source function has either decayed to zero at time-step $N_s$ or is switched off at time-step $N_s$—this could correspond to the time at which the simulation is terminated). Thus (3) can be written

$$F(\omega')=\sum_{q=0}^{N_s-1}f[q]e^{-j\omega' q}. \tag{4}$$

For the sake of illustration, consider a 1-D computational domain in which the source-function $f[q]$ represents the time-varying field at some point. Further assume this field is propagating in the positive $x$ direction. The field at a point which is $m$ spatial steps away from where $f[q]$ is measured would be given by

$$f[m,q] = \frac{1}{2\pi}\int_0^{2\pi} F(\omega')e^{-j\tilde{k}\delta m}e^{j\omega' q}d\omega' \tag{5}$$

where $\tilde{k}$ is the numeric wavenumber and $\delta$ is the spatial step size. Equation (5) is the 1-D FDTD analog of (1). In one dimension a closed-form expression can be obtained for $\tilde{k}\delta$

$$\tilde{k}\delta = 2\sin^{-1}\left(\frac{1}{S_c}\sin\left(\frac{\omega'}{2}\right)\right) \tag{6}$$

where $S_c$ is the Courant number. [One can equate $\omega'$ with the more familiar $\omega\Delta_t$ which typically appears in the FDTD dispersion relation, but the fact remains that $\omega'$ varies continuously in the integral of (5).]

Knowing the direction of propagation and the incident field at a given point (i.e., $f[q]$), one can calculate $F(\omega')$ using (4) and then find the field at an arbitrary point $f[m,q]$ using (5). This was done in [15] where it was shown how this approach could predict the superluminal component of FDTD propagation. It was speculated in [15] that this technique could be used to realize a TFSF boundary which would essentially be perfect. Indeed, this approach is at the core of the work by [4] and [5], but neither paper provided details concerning the Fourier transforms nor were details discussed in [15]. (It should also be pointed out that Ma *et al.* [16] have obtained an analytic expression for the field at an arbitrary point in the FDTD grid due to a source which is impulsive both in time and space. That differs from the solution here in that plane waves are of interest. These plane waves may be impulsive in time but cannot, by definition, be impulsive in more than one direction.)

Substituting (3) (after a change of index from $q$ to $q'$) into (5) and rearranging yields

$$f[m,q] = \sum_{q'=0}^{N_s-1} f[q']\frac{1}{2\pi}\int_0^{2\pi} e^{-j\tilde{k}\delta m}e^{j\omega'(q-q')}d\omega'. \tag{7}$$

This equation is exact and the integral possesses some interesting properties (for example, it is zero when $m > (q-q')$). Note that the source function $f[q']$ is assumed to be zero for $q' \geq N_s$ but $f[m,q]$ can be evaluated for any value of $q$, i.e., it is not bound by $N_s$. Unfortunately this equation cannot be easily evaluated efficiently nor can it be evaluated without resorting to numerical approximations.

An efficient calculation of this expression is obtained by employing standard discrete Fourier techniques (as was done in [4], [5], [15]). This is equivalent to approximating the integral in (5) as a Riemann sum. Let us assume that $N_t$ equally spaced samples of the integrand are used to approximate the integral. In this case the frequency $\omega'$ is given by $2\pi n/N_t$ (where $0 \leq n \leq N_t - 1$) and $d\omega'$ is approximately $2\pi/N_t$. An approximation of (5) is thus

$$f[m,q] \approx \frac{1}{2\pi}\sum_{n=0}^{N_t-1} F\left(\frac{2\pi n}{N_t}\right)e^{-j\tilde{k}\delta m}e^{j\frac{2\pi n}{N_t}q}\frac{2\pi}{N_t}. \tag{8}$$

Regrouping terms and employing (4) yields

$$f[m,q] \approx \sum_{n=0}^{N_t-1}\left\{\frac{1}{N_t}\sum_{q'=0}^{N_s-1} f[q']e^{-j\frac{2\pi n}{N_t}q'}\right\}e^{-j\tilde{k}\delta m}e^{j\frac{2\pi nq}{N_t}}. \tag{9}$$

If one sets $N_s$ equal to $N_t$ (which can be accomplished by zero-padding the source function $f[q']$ to the necessary length), then the term within braces is recognized as the discrete Fourier transform of the source function. This transform is multiplied by $\exp(-j\tilde{k}\delta m)$ and then the inverse discrete Fourier transform is taken. Since discrete Fourier transforms can be calculated efficiently, (9) can be calculated efficiently.

In the implementation of a TFSF boundary, one must calculate fields which are offset both spatially and temporally. Even though two fields are temporally offset by half a time step they still use identical samples of the source function $f[q']$. The offset is accounted for in the inverse transform, i.e.

$$\begin{aligned} f\left[m+\frac{1}{2}, q+\frac{1}{2}\right] &= \sum_{n=0}^{N_t-1} F(\omega_n)e^{-j\tilde{k}\delta(m+\frac{1}{2})}e^{j\frac{2\pi n(q+1/2)}{N_t}} \\ &= \sum_{n=0}^{N_t-1} F(\omega_n)e^{-j\tilde{k}\delta/2}e^{j\frac{\pi n}{N_t}}e^{-j\tilde{k}\delta m}e^{j\frac{2\pi nq}{N_t}} \end{aligned} \tag{10}$$

where $F(\omega_n)$ is the term in braces in (9). (When calculating the various field components one must also account for the characteristic impedance and the orientation of the fields. This is discussed more later.)

One question which remains is the value which should be chosen for $N_t$ to obtain a good approximation of the exact integral. Naturally, the more points the better the approximation will be, but one can obtain rough guidelines as follows. Using discrete transforms is equivalent to assuming the source function is periodic. However, one does *not* want this periodic behavior to be evident in the simulation. Hence the discrete Fourier transforms must be long enough (i.e., $N_t$ must be great enough) so that virtually all the energy associated with the incident field has traversed the total-field region before the incident field can repeat itself.

For example, consider an incident pulse which is non-zero for 100 time-steps ($N_s = 100$) and which is incident upon a TF region which is 50 spatial steps wide. The inverse transform associated with the last point in the TF region must be sufficiently long so that it can model the time it takes for the incident pulse to propagate to that point and the time it takes for the pulse to completely pass this point. Although the pulse started

by being bound by 100 time steps, because of the dispersion in the FDTD grid, it will take more than 100 time steps for the pulse to pass any point. The more distance the pulse has to travel, the more it will disperse. In fact, as discussed in [5], [17], [18], the group velocity in the FDTD grid goes to zero at the coarsest discretizations and hence it arguably takes an infinite time for a pulse to pass completely any point. Nevertheless, in practical applications the coarsest discretization are not of interest. By using a reasonable Courant number and a reasonable discretization of the incident pulse, there will be little spectral content at the coarsest discretization. Thus, in this example, a discrete Fourier transforms of 1024 points (i.e., $N_t = 1024$) would almost certainly be sufficient to describe the incident pulse over the entire TFSF boundary.

The FDTD simulation itself can proceed for any number of time steps. If a highly resonant structure were being illuminated and the user wanted to run the simulation for a hundred-thousand time steps, or more, that would be irrelevant to the implementation of the TFSF boundary. The incident field on the boundary would merely be assumed to be zero after 1024 time steps.

Generalizing (5) to higher dimensions is trivial in that it is nearly identical to (1)—the only differences are the limits of the integral and the use of the discrete wavenumber components. For example, assuming a uniform grid in which $\Delta_x = \Delta_y = \delta$, let the field $f[m, n, q]$ represent the fields at the point $\mathbf{r} = (m\delta, n\delta)$ and time $q\Delta_t$. Given the field $f[q]$ at the origin which has Fourier transform $F(\omega')$, $f[m, n, q]$ is given by

$$f[m,n,q] = \frac{1}{2\pi}\int_0^{2\pi} F(\omega')e^{-j\tilde{\mathbf{k}}\cdot\mathbf{r}}e^{j\omega' q}d\omega'. \qquad (11)$$

In this case the components of the numeric wave vector $\tilde{\mathbf{k}}$ must be calculated from the 2-D dispersion relation but the integral can again be approximated with discrete transforms as done in (9). We note that the superluminal wave vector components discussed in [15], [19] are not incorporated in the results to be shown later. These components, which occur at the coarsest discretizations supported by the grid, experience exponential decay as they propagate. Discarding them from the solution slightly increases the amount of leaked fields but this is not a concern in practice (owing to the associated frequencies not being ones which would be of interest and the inherent exponential decay).

Equation (5) gives the spatial and temporal dependence of a single field component. Given a single field component, the polarization, and the direction of propagation, all the other field components can be computed. Despite the characteristic impedance of the FDTD grid being exact, such a computation is more involved than in the continuous world because of the non-orthogonality of the electric field, magnetic field, and wave vector. Details of the relationship between these three quantities are discussed in [5].

When a halfspace discontinuity is present, one must account for the reflected or, where applicable, the transmitted fields. To demonstrate this, we first consider the case of illumination of a PEC plane where there is no transmitted field and the reflection coefficient is $-1$. We then consider penetrable media which must incorporate the transmission and reflection coefficients.

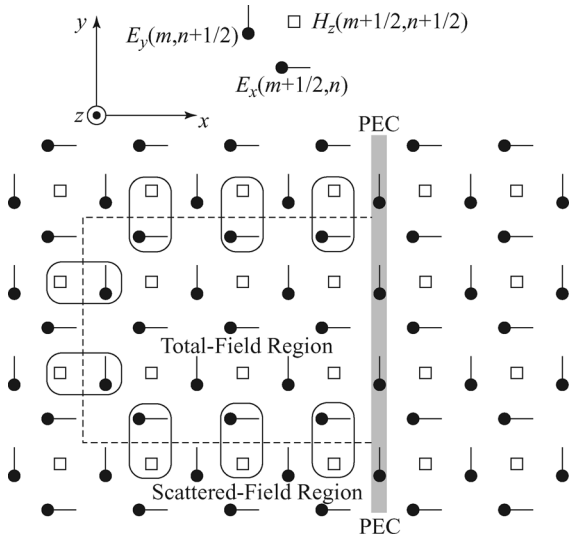


Fig. 1. Depiction of a $\mathrm{TE}^z$ grid containing a PEC plane. The TFSF boundary is drawn with a dashed lines. The nodes enclosed in rounded rectangles must have their values corrected owing to a neighboring node being on the other side of the boundary.

## III. $\mathrm{TE}^z$ Polarization and a PEC Plane

Consider a 2-D FDTD grid with $\mathrm{TE}^z$ polarization in which a PEC plane is assumed, at least insofar as the incident field is concerned, to span the computational domain. This scenario is depicted in Fig. 1. We define the "incident field" as being the sum of the incoming field (i.e., the field whose $x$-component of the wave vector is positive) and the reflected field. By doing this, in the absence of any additional scatterers other than the PEC plane itself, the SF region would contain no fields. It is important to note that in any given simulation there are no restrictions on the contents of the TF region. In fact, the PEC plane does not even have to span the TF region. Thus, for example, one can consider the fields associated with obliquely illuminated apertures. In the SF region, however, it is required that the plane is intact and that no other scatterers are present.

Nodes which are tangential to the TFSF boundary and have a neighboring node on the other side of the boundary must have their update-equations corrected to account for the existence of the TFSF boundary (see [2] for details). For the situation considered here, the TFSF boundary is only three-sided. The field is not specified on, or beyond, the PEC. Instead, as is usual when modeling PECs, the tangential electric fields along the PEC are set to zero and the FDTD algorithm handles the rest.

To implement the TFSF method, the incident field contains two plane waves: the "incoming field" and the reflected field. This scenario is shown in Fig. 2. The "reference point" in Fig. 2 is essentially the origin at which the user would specify the source function $f[q]$. Note that this point does not need to be within the computational domain! Its location is on the PEC and such that for the given incident angle $\phi_i$ at the start of the simulation the incoming field has not yet entered the TF region (but

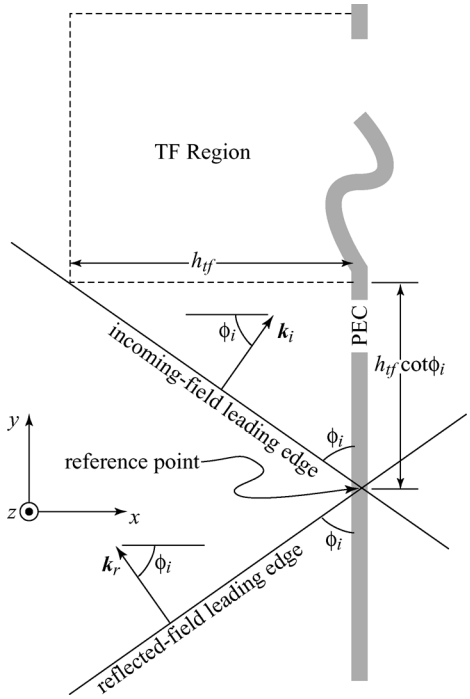


Fig. 2. To model a PEC boundary, the "incident field" contains both an incoming and a reflected field. The width of the TF region is $h_{tf}$. The origin, or reference point, for the sake of calculating the incident field is a distance $h_{tf}\cot(\phi_i)$ from the bottom of the TF region. This ensures that the incoming field, which is specified by the source function $f[q]$, is completely outside of the TF region at the start of the simulation. The bending of, and gap in, the PEC boundary is used to emphasize that there are no restrictions on the contents of the TF region. Inhomogeneities can be present throughout the region.

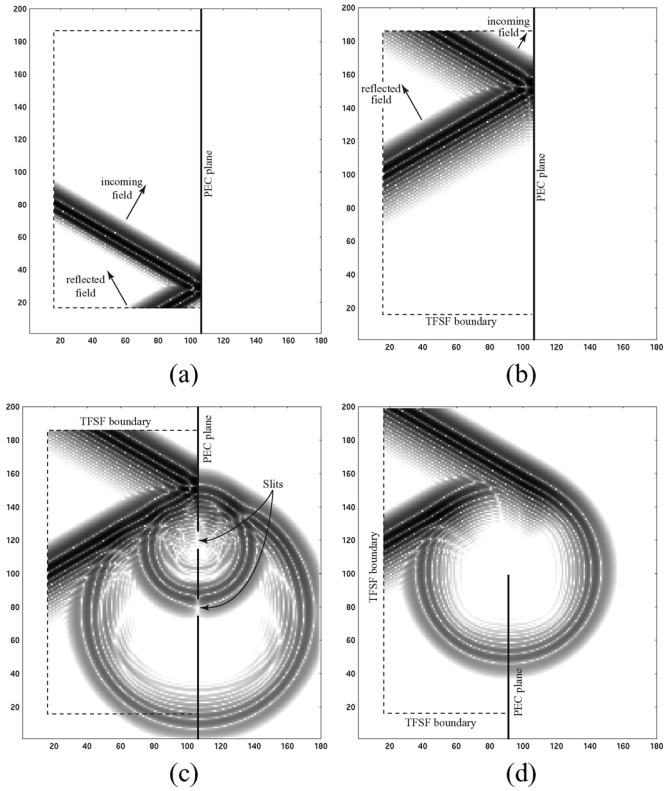


Fig. 3. Snapshots of the magnetic field at time-steps (a) 150 and (b) 350. (c) Magnetic field at time-step 350 when two slits are present in the PEC plane. (d) Magnetic field at time-step 350 showing diffraction from the edge of a semi-infinite plane. The incident angle is 60 degrees with respect to horizontal.

the leading edge of the field sits poised to enter the region). The field at points along the TFSF boundary are then determined relative to displacement from this reference point in accordance with (11).

One can easily show that the FDTD reflection coefficient for a PEC plane is identically $-1$ (relative to the electric field) and the details will not be presented here. Suffice it to say that the incoming and reflected fields have the same $y$ components of their wave numbers and equal magnitude but opposite signs for the $x$ components. The Fourier transform of the source function $f[q]$ is taken to be the spectral representation of the magnetic field for both the incoming and reflected fields. The $x$ and $y$ components of the electric field are found in accordance with the orthogonality condition discussed in [5]. (The incoming and reflected fields have the same sign for the $x$ component of the electric field but opposite signs for the $y$ component.) Thus the incident field is realized by summing two plane waves, each with a common reference point and the same amplitude. The only difference is the direction of propagation. The calculation of each individual plane wave follows the details provided in [5]. The superposition of these waves satisfies the boundary condition dictated by the existence of a PEC plane in the FDTD grid and hence can be used to realize a nearly perfect TFSF boundary.

To illustrate the behavior of this TFSF implementation, consider a pulsed plane wave propagating at an incident angle of 60 degrees. The field is traveling in free space and the Courant number is 95 percent of the 3-D limit, i.e., $S_c = 0.95/\sqrt{3}$. This Courant number was chosen so that the results pertain to 3-D simulations in which the incident field propagates orthogonal to one of the axes (the factor of 95 percent was chosen somewhat arbitrarily—stability is no more of a concern with this TFSF technique than it is with the surrounding grid). The pulse is a Ricker wavelet discretized so that there are 10 cells per wavelength at the most energetic frequency. At this discretization there is a substantial amount of energy at coarser discretization (see [5] for further discussion of this source function). One would anticipate this pulse would suffer substantial dispersion as it propagates, something which is undesirable in practice but good for testing the performance of a TFSF implementation. Fig. 3 shows a computational domain which is 180 by 200 cells. A vertical PEC exists 105 cells from the left. The SF region is 15 cells thick. Fig. 3(a) shows the magnetic field 150 time-steps into the simulation. The images show the log base 10 of the absolute value of the field and have been scaled so that it is visible over three orders of magnitude. In Fig. 3(a) the incoming field has already encountered the PEC. The TFSF boundary is aware of the reflected field and there is virtually no leakage through the boundary. Fig. 3(b) shows the magnetic field at 350 time steps. The dispersion of the incoming field is clearly evident as the width of the pulse is greater than it had been at 150 time-steps. This dispersion is subsequently evident in the field reflected by the PEC plane. The AFP TFSF implementation automatically incorporates these numeric artifacts. Using a discrete Fourier transform of 1024 points, the peak magnetic field leaked across the boundary in this case is approximately five orders of magnitude down from the peak value of the magnetic field (i.e., 100

dB down from the peak). If one were to use a more reasonable discretization of 20 cells per wavelength at the peak frequency of the pulse, the leaked field drops to 180 dB down from the peak of the incident field. (Note that in Fig. 3(a) and (b) there is no reason to extend the computational domain beyond the PEC boundary since no fields propagate past the PEC. It was done here merely for the sake of consistency with (c) and (d).)

Fig. 3(c) also shows the magnetic field over the computational domain at time-step 350, but in this case there are two slits in the PEC plane. Each slit is 10 cells wide and their centers are separated by 40 cells. The field scattered back to the left of the PEC as well as the field which passes through the slits are clearly evident. The implementation of the TFSF boundary is oblivious to the actual contents of the TF region (or to anything beyond the PEC plane).

The diffraction from infinite wedges was studied using the FDTD method in [20], [21]. In that work the TFSF boundary passed through the perfectly matched layer (PML) which terminated the grid. For a field originating in the PML, an amplification factor had to be found to compensate for the PML loss. Using the AFP TFSF technique, it would not be necessary to have an incoming field start within the PML owing to the fact that the AFP TFSF technique already includes the reflected field. This is illustrated in Fig. 3(d) which shows the diffraction from a "knife edge." This snapshot is also of the magnetic field and at time-step 350. In this case the TFSF boundary is two-sided. One-side, which is drawn vertically, is terminated one cell before the top edge of the computational domain where a second-order Higdon ABC is used. The grid termination would benefit from the use of a PML as described in [20], [21], but no amplification factors would be needed and the reflected field would be completely present at the start of the TFSF boundary. Thus the reflected field would not have to build up from the start of the PEC plane which is within the PML nor would it suffer the corresponding diffraction at that leading edge—there is no "leading edge" of the PEC in the AFP TFSF implementation for the incoming field to encounter. Instead of the knife-edge shown here, wedges could be studied just as easily (and, as will be more clear after considering dielectric boundaries, the technique can be applied to penetrable wedges too).

The AFP TFSF technique allows the calculation of the incoming and/or the reflected field at an arbitrary point. The technique does not care if the point is actually on the TFSF boundary or even if it is within the grid. Thus, when it comes to recording, for example, the diffracted field, the observation points can be placed anywhere in the computational domain. One can subtract the incident or reflected field from the recorded field. In this way, one does not have to restrict observation points to the scattered-field region.

There are other problems which could benefit from the application of the AFP TFSF boundary described here. For example, it provides an alternative way to study the scattering from randomly rough surfaces than the one presented in [22]. In [22] the incident field employed a Gaussian-tapered plane wave as described in [23]. The Gaussian taper was necessary to minimize diffraction errors which would be present if an obliquely incident plane wave were to encounter a finite surface—only a finite amount of the rough surface can be included in any particular simulation. A Gaussian-tapered plane wave is not a true solution to the wave equation. Additionally, the taper is such that a very large computational domain must be used to ensure the fields are small at either end of the tapered wave. On the other hand, using the TFSF implementation described here, the surface is effectively infinite (although the surface roughness must be contained within the TF region). The surface roughness would have to be "turned on" (i.e., ramped up and down so that it met the edges of the planar surface at the TFSF boundary), but this can be done in much less space than the Gaussian tapering of the incident plane wave. Unlike with a Gaussian-tapered incident field, in the AFP TFSF method the incident field is a solution to the wave equation. Thus the AFP TFSF boundary has the potential to provide much more efficient and more accurate solutions to these types of problems.

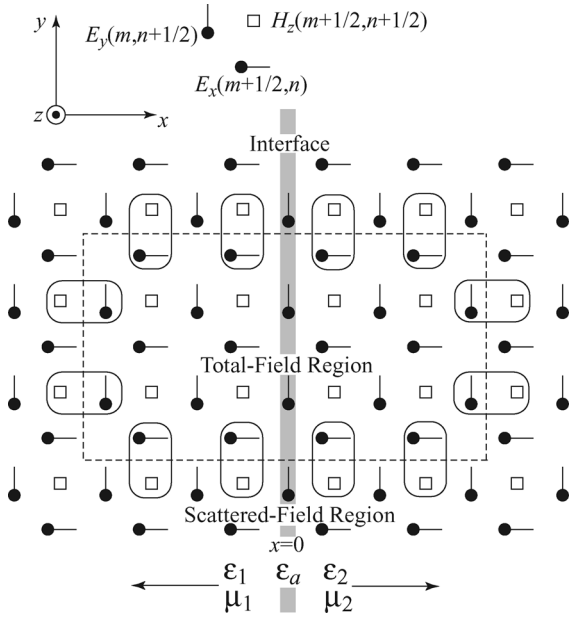


Fig. 4. Portion of the $\mathrm{TE}^z$ grid. An interface exists at $x = 0$. To the left of the interface the permittivity and permeability are $\epsilon_1$ and $\mu_1$, respectively, and to the right they are $\epsilon_2$ and $\mu_2$. Along the interface the permittivity is $\epsilon_a$. Magnetic fields are unambiguously in the first or second medium and hence always use either $\mu_1$ or $\mu_2$.

## IV. $\mathrm{TE}^z$ Polarization With a Dielectric Halfspace

For a field incident on a penetrable halfspace, one must account for both the reflected and transmitted fields and hence must know the reflection and transmission coefficients. Consider a plane wave propagating obliquely in the 2-D $\mathrm{TE}^z$ grid shown in Fig. 4. The non-zero fields are $E_x$, $E_y$, and $H_z$ (this corresponds to the polarization identified as TM in [4]). For the sake of simplicity, assume a uniform grid where $\Delta_x = \Delta_y = \delta$. The computational domain consists of two half-spaces where the permittivity and permeability are $\epsilon_1$ and $\mu_1$, respectively, to the left of the interface at $x = 0$ and $\epsilon_2$ and $\mu_2$ to the right. Throughout the following a subscript 1 will be used to indicate quantities to the left of the interface and a subscript 2 will indicate quantities to the right. The $E_y$ nodes along the interface have a permittivity of $\epsilon_a$, the value of which is left arbitrary for now.

We adopt the discrete calculus notation described in [5] (which differs slightly from that use in [4]) and start with the description of an arbitrary harmonic wave. The magnetic field is given by

$$\begin{aligned}\hat{\mathbf{H}} &= \mathbf{a}_z \hat{H}_z = \mathbf{a}_z \hat{H}_0 e^{-j(\tilde{k}_x m\delta + \tilde{k}_y n\delta)} e^{j\omega q \Delta_t} \\ &= \mathbf{a}_z \hat{H}_0 e^{-j\tilde{\mathbf{k}}\cdot\mathbf{r}} e^{j\omega q\Delta_t} \end{aligned} \tag{12}$$

where, for propagation at an angle $\phi$ relative to the $x$ axis, the numeric wave vector $\tilde{\mathbf{k}}$ is

$$\tilde{\mathbf{k}} = (\tilde{k}_x, \tilde{k}_y) = \tilde{k}(\cos\phi, \sin\phi) \tag{13}$$

$\omega$ is the frequency, $q$ is the temporal index, and $m$ and $n$ are the spatial indices in the $x$ and $y$ directions, respectively. The spatial dependence is given by $\exp(-j\tilde{\mathbf{k}}\cdot\mathbf{r})$ where $\mathbf{r} = (m\delta, n\delta)$ ($m$ and $n$ are not restricted to integer values and can be offset by appropriate fractional amounts to account for the staggering of the grid). The corresponding electric field is given by

$$\begin{aligned}\hat{\mathbf{E}} &= \mathbf{a}_x \hat{E}_x + \mathbf{a}_y \hat{E}_y = (\mathbf{a}_x \hat{E}_{0x} + \mathbf{a}_y \hat{E}_{0y}) e^{-j\tilde{\mathbf{k}}\cdot\mathbf{r}} e^{j\omega q\Delta_t} \\ &= \hat{\mathbf{E}}_0 e^{-j\tilde{\mathbf{k}}\cdot\mathbf{r}} e^{j\omega q\Delta_t}. \end{aligned} \tag{14}$$

The vector $\tilde{\mathbf{k}}$ and scalar $\hat{H}_0$ are constants for a given frequency (but are themselves functions of frequency). A tilde indicates a numeric quantity while a caret implies a quantity is in the frequency domain and may be complex.

Let the shift operator $s_\xi^+$ shift the $\xi$-index by $+1/2$ where $\xi \in \{x, y, t\}$. For example

$$s_x^+ \hat{\mathbf{E}} = \hat{\mathbf{E}}_0 e^{-j(\tilde{k}_x(m+1/2)\delta + \tilde{k}_y n\delta)} e^{j\omega q\Delta_t} = e^{-j\tilde{k}_x\delta/2}\hat{\mathbf{E}}. \tag{15}$$

Conversely, $s_\xi^-$ shifts the $\xi$-index by $-1/2$. The discrete difference operator $\tilde{\partial}_\xi$ is defined as

$$\tilde{\partial}_\xi = \frac{1}{\Delta_\xi}\left(s_\xi^+ - s_\xi^-\right). \tag{16}$$

For plane-wave propagation, the discrete difference operators can be represented by multiplicative functions. When $\xi$ is either $x$ or $y$ one obtains

$$\tilde{\partial}_\xi \hat{\mathbf{E}} = -j\frac{2}{\delta}\sin\left(\frac{\tilde{k}_\xi\delta}{2}\right)\hat{\mathbf{E}} = -jK_\xi\hat{\mathbf{E}}. \tag{17}$$

Similarly, the temporal finite difference yields

$$\tilde{\partial}_t \hat{\mathbf{E}} = j\frac{2}{\Delta_t}\sin\left(\frac{\omega\Delta_t}{2}\right)\hat{\mathbf{E}} = j\Omega\hat{\mathbf{E}}. \tag{18}$$

The difference operators acting on the magnetic field yield similar results. In terms of these operators the dispersion relationship is given by

$$\Omega^2\mu\epsilon = K_x^2 + K_y^2. \tag{19}$$

Ignoring the shift operators which are common to both sides, for the two-dimensional propagation which pertains here, the FDTD harmonic form of Ampere's law can be written

$$j\Omega\epsilon\hat{\mathbf{E}} = -j\mathbf{K}\times\hat{\mathbf{H}} = -j\mathbf{a}_x K_y \hat{H}_z + j\mathbf{a}_y K_x \hat{H}_z \tag{20}$$

where $\mathbf{K} = (K_x, K_y)$ (see [5] for further details including the shift operators which have been dropped). Thus, the components of the electric field are related to the magnetic field via

$$\hat{E}_x = -\frac{K_y}{\Omega\epsilon}\hat{H}_z \tag{21}$$

$$\hat{E}_y = \frac{K_x}{\Omega\epsilon}\hat{H}_z. \tag{22}$$

As mentioned previously, knowing one field component, the polarization, and the direction of propagation, one can obtain all the field components. Equations (21) and (22) demonstrate this is true.

To solve for the reflection and transmission coefficients, one must obtain two independent equations relating them. As in the continuous world, the phase of the incoming, reflected, and transmitted fields must match along the interface. This dictates that the angle of reflection must equal the angle of incidence. Assuming a unit amplitude incoming wave, the incoming, reflected, and transmitted magnetic fields can be written, respectively

$$\hat{\mathbf{H}}^i = \mathbf{a}_z e^{-j\tilde{\mathbf{k}}_i\cdot\mathbf{r}} \tag{23}$$

$$\hat{\mathbf{H}}^r = -\mathbf{a}_z\hat{\tilde{\Gamma}}_{te} e^{-j\tilde{\mathbf{k}}_r\cdot\mathbf{r}} \tag{24}$$

$$\hat{\mathbf{H}}^t = \mathbf{a}_z\hat{\tilde{T}}_{te} e^{-j\tilde{\mathbf{k}}_t\cdot\mathbf{r}} \tag{25}$$

where

$$\tilde{\mathbf{k}}_i = \mathbf{a}_x\tilde{k}_1\cos\phi_i + \mathbf{a}_y\tilde{k}_1\sin\phi_i = (\tilde{k}_{1x}, \tilde{k}_y) \tag{26}$$

$$\tilde{\mathbf{k}}_r = -\mathbf{a}_x\tilde{k}_1\cos\phi_i + \mathbf{a}_y\tilde{k}_1\sin\phi_i = (-\tilde{k}_{1x}, \tilde{k}_y) \tag{27}$$

$$\tilde{\mathbf{k}}_t = \mathbf{a}_x\tilde{k}_2\cos\phi_t + \mathbf{a}_y\tilde{k}_2\sin\phi_t = (\tilde{k}_{2x}, \tilde{k}_y) \tag{28}$$

$\tilde{k}_1$ and $\tilde{k}_2$ are the FDTD wave numbers in the first and second media, respectively, $\phi_i$ is the incident angle, $\phi_t$ is the transmitted angle, and $\hat{\tilde{\Gamma}}_{te}$ and $\hat{\tilde{T}}_{te}$ are the reflection and transmission coefficients, respectively. The temporal dependence which is common to all terms has been dropped. Because of the phase matching which must exist at the interface, $\tilde{k}_1\sin\phi_i$ must equal $\tilde{k}_2\sin\phi_t$, i.e., the $y$ component of the wave vector is the same throughout the grid.

The total field in the first medium is the sum of the incoming and reflected waves, i.e.

$$\hat{\mathbf{H}}_1 = \mathbf{a}_z(e^{-j\tilde{\mathbf{k}}_i\cdot\mathbf{r}} - \hat{\tilde{\Gamma}}_{te}e^{-j\tilde{\mathbf{k}}_r\cdot\mathbf{r}}) \tag{29}$$

$$\hat{\mathbf{E}}_1 = -\frac{\mathbf{K}^i}{\Omega\epsilon_1}\times\mathbf{a}_z e^{-j\tilde{\mathbf{k}}_i\cdot\mathbf{r}} + \frac{\mathbf{K}^r}{\Omega\epsilon_1}\times\mathbf{a}_z\hat{\tilde{\Gamma}}_{te}e^{-j\tilde{\mathbf{k}}_r\cdot\mathbf{r}}. \tag{30}$$

The total field in the second medium is given by the transmitted field. The transmitted electric field is

$$\hat{\mathbf{E}}^t = -\frac{\mathbf{K}^t}{\Omega\epsilon_2}\times\mathbf{a}_z\hat{\tilde{T}}_{te}e^{-j\tilde{\mathbf{k}}_2\cdot\mathbf{r}}. \tag{31}$$

The vectors $\mathbf{K}^i$, $\mathbf{K}^r$, and $\mathbf{K}^t$ are given by $(K_{1x}, K_y)$, $(-K_{1x}, K_y)$ and $(K_{2x}, K_y)$, respectively. Because the tangential phase is the same for all the fields, it is also true that $K_y$ is the same for all the fields.

Note that only $E_y$ nodes are present at the interface. Nevertheless, as in the continuous world, the tangential electric field must match at the interface, i.e.

$$\mathbf{a}_y\cdot\hat{\mathbf{E}}_1|_{x=0} = \mathbf{a}_y\cdot\hat{\mathbf{E}}^t|_{x=0}. \tag{32}$$

Expanding these terms yields

$$\frac{K_{1x}}{\Omega\epsilon_1}e^{-j\tilde{k}_1\sin(\phi_i)y} + \frac{K_{1x}}{\Omega\epsilon_1}\hat{\tilde{\Gamma}}_{te}e^{-j\tilde{k}_1\sin(\phi_i)y} = \frac{K_{2x}}{\Omega\epsilon_2}\hat{\tilde{T}}_{te}e^{-j\tilde{k}_2\sin(\phi_t)y}. \tag{33}$$

Because the phase must match along the boundary, the complex exponential can be eliminated. Canceling $\Omega$ this equation can be written

$$1 + \hat{\tilde{\Gamma}}_{te} = \frac{\epsilon_1}{\epsilon_2}\frac{K_{2x}}{K_{1x}}\hat{\tilde{T}}_{te}. \tag{34}$$

Another equation relating the reflection and transmission coefficients can be obtained from the update-equation for the electric-field nodes on the interface. The relevant equation is the $y$ component of Ampere's law evaluated at $x = 0$. This was given in (20) but that assumed propagation in a homogeneous space which is no longer pertinent. Instead, we explicitly write the spatial finite difference

$$j\Omega\epsilon_a\hat{E}_y|_{x=0} = -\tilde{\partial}_x\hat{H}_z|_{x=0} = -\frac{1}{\delta}\left(\hat{H}_z^t\Big|_{x=\delta/2} - \hat{H}_{1z}\Big|_{x=-\delta/2}\right). \tag{35}$$

Unlike before, the spatial finite difference operator $\tilde{\partial}_x$ cannot be expressed directly in terms of $K$'s since the difference involves fields on either side of the interface. The electric field in (35) can be represented as either the transmitted field or the sum of the incoming and reflected fields—the same result will ultimately be obtained. Using the transmitted field for the electric field and discarding common phase terms yields

$$j\Omega\epsilon_a\frac{K_{2x}}{\Omega\epsilon_2}\hat{\tilde{T}}_{te} = -\frac{1}{\delta}\left(\hat{\tilde{T}}_{te}e^{-j\kappa_{2x}} - [e^{j\kappa_{1x}} - \hat{\tilde{\Gamma}}_{te}e^{-j\kappa_{1x}}]\right) \tag{36}$$

where

$$\kappa_{1x} = \frac{\tilde{k}_1\cos(\phi_i)\delta}{2}, \tag{37}$$

$$\kappa_{2x} = \frac{\tilde{k}_2\cos(\phi_t)\delta}{2}. \tag{38}$$

Combining (34) and (36) and solving for the reflection coefficient yields

$$\hat{\tilde{\Gamma}}_{te} = \frac{\frac{K_{2x}}{\epsilon_2}e^{j\kappa_{1x}} - \frac{K_{1x}}{\epsilon_1}e^{-j\kappa_{2x}} - j\frac{\epsilon_a}{\epsilon_1\epsilon_2}K_{1x}K_{2x}\delta}{\frac{K_{2x}}{\epsilon_2}e^{-j\kappa_{1x}} + \frac{K_{1x}}{\epsilon_1}e^{-j\kappa_{2x}} + j\frac{\epsilon_a}{\epsilon_1\epsilon_2}K_{1x}K_{2x}\delta}. \tag{39}$$

As the discretization goes to zero, the third term in the numerator and denominator goes to zero, the complex exponentials approach one, and the $K_x$'s approach the $x$ component of the wavenumber in their respective media. Thus this expression gives the continuous-world reflection coefficient as the discretization goes to zero. It is interesting to note that this is true even though at this point we have placed no restrictions on $\epsilon_a$, the permittivity used for the nodes along the interface (although inherent in the derivation is the restriction that $\epsilon_a$ cannot be a pathological value such as zero).

Using (34) in (39), the transmission coefficient is found to be

$$\hat{\tilde{T}}_{te} = \frac{2\frac{K_{1x}}{\epsilon_1}\cos(\kappa_{1x})}{\frac{K_{2x}}{\epsilon_2}e^{-j\kappa_{1x}} + \frac{K_{1x}}{\epsilon_1}e^{-j\kappa_{2x}} + j\frac{\epsilon_a}{\epsilon_1\epsilon_2}K_{1x}K_{2x}\delta}. \tag{40}$$

Using Euler's formula to expand the complex exponentials and writing the $K$'s in terms of sines, the reflection coefficient can be written

$$\hat{\tilde{\Gamma}}_{te} = \frac{\frac{\sin(\kappa_{x2})\cos(\kappa_{x1})}{\epsilon_2} - \frac{\sin(\kappa_{x1})\cos(\kappa_{x2})}{\epsilon_1} - j\aleph}{\frac{\sin(\kappa_{x2})\cos(\kappa_{x1})}{\epsilon_2} + \frac{\sin(\kappa_{x1})\cos(\kappa_{x2})}{\epsilon_1} + j\aleph} \tag{41}$$

where the imaginary term in the numerator and denominator is

$$\aleph = \frac{\sin(\kappa_{x1})\sin(\kappa_{x2})}{\epsilon_1\epsilon_2}(2\epsilon_a - \epsilon_1 - \epsilon_2). \tag{42}$$

Note that when $\epsilon_a$ is the average of the permittivities to either side of the interface $\aleph$ is zero. In this way the imaginary part of the reflection and transmission coefficients is zero. Since the continuous-world reflection and transmission coefficients are purely real, the imaginary part is an inherent error. The expressions above effectively constitute a proof that using the average permittivity for the interface nodes is optimum. For

$\epsilon_a = (\epsilon_1 + \epsilon_2)/2$ the reflection and transmission coefficients become

$$\hat{\tilde{\Gamma}}_{te} = \frac{\epsilon_1 \sin(\kappa_{x2})\cos(\kappa_{x1}) - \epsilon_2 \sin(\kappa_{x1})\cos(\kappa_{x2})}{\epsilon_1 \sin(\kappa_{x2})\cos(\kappa_{x1}) + \epsilon_2 \sin(\kappa_{x1})\cos(\kappa_{x2})} \quad (43)$$

$$\hat{\tilde{T}}_{te} = \frac{2\epsilon_2 \sin(\kappa_{x1})\cos(\kappa_{x1})}{\epsilon_1 \sin(\kappa_{x2})\cos(\kappa_{x1}) + \epsilon_2 \sin(\kappa_{x1})\cos(\kappa_{x2})}. \quad (44)$$

Despite the change in permeability, these equations are seemingly independent of permeability. However, the permeabilities dictate the wave numbers in the different media and hence the permeabilities are implicitly contained within these equations.

Reflection and transmission coefficients for this polarization were provided in [4, Eqs. (72) and (73)]. The reflection coefficient in that work involves the sum of 28 terms (these terms involve the product of a total of 17 complex exponentials and 30 sine functions) and was obtained with the aid of a computer algebra package. The complexity of that expression is, it must be noted, a consequence of Moss *et al.* considering more complex media than that assumed here. However, their final results do tend to obscure the simplicity which pertains to the problem of interest here. The reflection coefficients which pertain to PML interfaces have also been studied extensively. Derivations of the numeric PML reflection coefficient can be found in [24]–[27].

With the reflection and transmission coefficients known, the incident field can be calculated at an arbitrary point given the source function $f[q]$ at a reference point and the direction of propagation of the incident field. The location of the reference point is unchanged from that depicted in Fig. 2. Here we take the "incident field" to mean the sum of the incoming and reflected field if a node is to the left of the interface and the transmitted field if the node is to the right. Thus, the time-domain incident magnetic field for points to the left of the interface are given by

$$H_{1z}\left[m+\frac{1}{2}, n+\frac{1}{2}, q+\frac{1}{2}\right] = \mathcal{F}^{-1}\left[F(\omega)(e^{-j\tilde{\mathbf{k}}_i\cdot\mathbf{r}} - \hat{\tilde{\Gamma}}_{te}e^{-j\tilde{\mathbf{k}}_r\cdot\mathbf{r}})\right] \quad (45)$$

where $F(\omega) = \mathcal{F}[f[q]]$. As discussed in connection with (10), the offsets of 1/2 are accounted for in the inverse transforms. From (21) and (22), the $x$ and $y$ components of the electric field are

$$E_{1x}\left[m+\frac{1}{2}, n, q\right] = -\mathcal{F}^{-1}\left[\frac{K_y F(\omega)}{\Omega\epsilon_1}(e^{-j\tilde{\mathbf{k}}_i\cdot\mathbf{r}} - \hat{\tilde{\Gamma}}_{te}e^{-j\tilde{\mathbf{k}}_r\cdot\mathbf{r}})\right] \quad (46)$$

$$E_{1y}\left[m, n+\frac{1}{2}, q\right] = \mathcal{F}^{-1}\left[\frac{K_x F(\omega)}{\Omega\epsilon_1}(e^{-j\tilde{\mathbf{k}}_i\cdot\mathbf{r}} + \hat{\tilde{\Gamma}}_{te}e^{-j\tilde{\mathbf{k}}_r\cdot\mathbf{r}})\right]. \quad (47)$$

These expressions, as well as the corresponding expression for the transmitted fields, are evaluated for the points adjacent to the TFSF boundary.

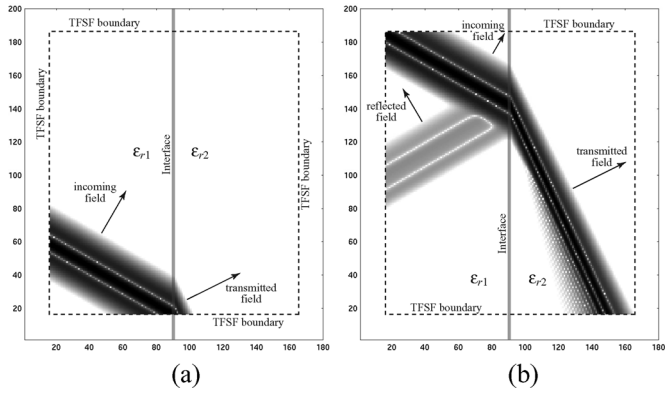


Fig. 5. Snapshots of the magnetic field at time-steps (a) 150 and (b) 350.

To illustrate the behavior of the TFSF boundary, Fig. 5 shows two snapshots of the magnetic field in a computational domain which is 180 by 200 cells. Free space is to the left and extends over 90 cells. To the right is a dielectric with a permittivity of $4\epsilon_0$ ($E_y$ nodes along the interface use a permittivity of $2.5\epsilon_0$). The permeability in both regions is that of free space. The incoming pulse is a Ricker wavelet discretized such that there are 20 cells per free-space wavelength at the most energetic frequency. This corresponds to 10 cells per wavelength in the dielectric. The SF region is 15 cells thick, the incident angle is 60 degrees, and the Courant number is $0.95/\sqrt{3}$.

Fig. 5(a) shows the $H_z$ field at 150 time steps when the leading edge of the pulse has first encountered the dielectric at the center of the bottom of the figure. Fig. 5(b) shows the field at 350 time steps. Now the reflected and transmitted field are clearly evident. Since no scatterer is present in this simulation, no scattered fields are visible in the SF region (the plot uses three decades of logarithmic scaling). One can clearly see the refraction of the transmitted field. Also, owing to the higher permittivity of the second medium, the transmitted field suffers more numeric dispersion than fields in the first medium. (Dispersion in the FDTD grid is dictated by the discretization [2]. The higher permittivity in the second medium results in shorter wavelengths, and hence coarser discretization and greater dispersion, than in the first medium.) The increased dispersion causes the transmitted pulse to broaden noticeably as it propagates—one can see that the pulse is thinest at the interface. One may ask why, at any given time step, the incoming way does not have a similar appearance to the transmitted field, i.e., thinner to the left and thicker to the right? The answer is that the incident field along the TFSF boundary is exactly matching the phase speed for all the spectral components for the particular incident angle, i.e., all spectral components have the same $\phi_i$. At the interface between free space and the dielectric, boundary conditions dictate the fields must be continuous. However, the free-space phase speeds are not matched to the phase speeds in the dielectric so as to yield a single transmitted angle. Since the phase speeds are a function of the frequency, this causes the depth-dependent broadening (or thought of another way, the frequency-dependent refraction where $\phi_t$ is a function of frequency).

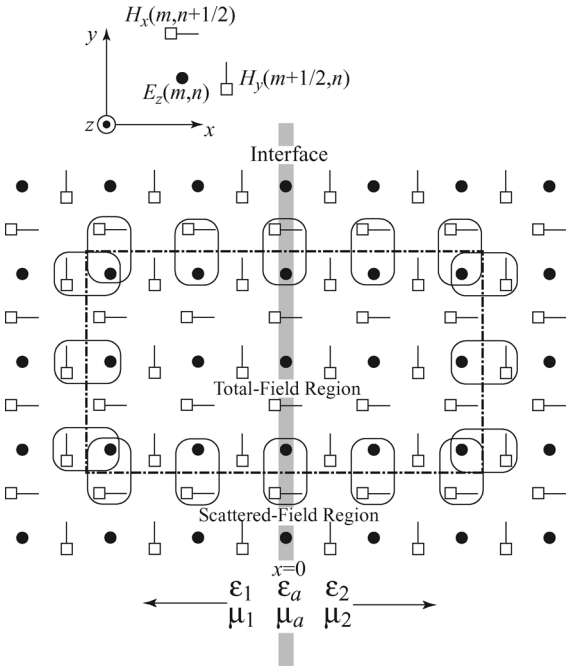


Fig. 6. Depiction of a $\mathrm{TM}^z$ grid with two dielectric halfspaces.

As with the PEC simulation, the leaked fields are approximately 100 dB down from the peak interior fields. When a more reasonable discretization is used (i.e., there is not significant energy with discretizations less than 10 cells per wavelength in the second medium), the peak leaked fields are more than 180 dB down from the peak of the incident field.

## V. $\mathrm{TM}^z$ Polarization With a Dielectric Halfspace

Consider the $\mathrm{TM}^z$ grid shown in Fig. 6. The interface is aligned with $H_x$ and $E_z$ nodes. The arrangement and indexing of nodes is consistent with the $\mathrm{TE}^z$ grid in that both grids could be considered slices of a 3-D grid where magnetic-field nodes are centered on the faces of the Yee cube while electric-field nodes are centered on the edges. For this polarization both electric- and magnetic-field nodes lie on the interface. The permittivity and permeability associated with these nodes is $\epsilon_a$ and $\mu_a$, respectively, which are left arbitrary for now. We again wish to find the reflection and transmission coefficients. The incoming, reflected, and transmitted electric field are given by, respectively,

$$\hat{\mathbf{E}}^i = \mathbf{a}_z e^{-j\tilde{\mathbf{k}}_i\cdot\mathbf{r}} \tag{48}$$

$$\hat{\mathbf{E}}^r = \mathbf{a}_z \hat{\tilde{\Gamma}}_{tm} e^{-j\tilde{\mathbf{k}}_r\cdot\mathbf{r}} \tag{49}$$

$$\hat{\mathbf{E}}^t = \mathbf{a}_z \hat{\tilde{T}}_{tm} e^{-j\tilde{\mathbf{k}}_t\cdot\mathbf{r}}. \tag{50}$$

where $\hat{\tilde{\Gamma}}_{tm}$ and $\hat{\tilde{T}}_{tm}$ are the $\mathrm{TM}^z$ reflection and transmission coefficients, respectively. Temporal dependence is given by $\exp(j\omega q\Delta_t)$ and is common to all terms (hence it is not shown explicitly). The definitions of other terms are as before. The FDTD form of Ampere's law is

$$j\Omega\epsilon\hat{E}_z = \tilde{\partial}_x\hat{H}_y - \tilde{\partial}_y\hat{H}_x. \tag{51}$$

Because, for the assumed geometry, the phase dependence in the $y$ direction is the same throughout the grid, $\tilde{\partial}_y$ can be replaced with $-jK_y$. For any of the fields, the FDTD form of Faraday's relates the electric and magnetic fields via

$$-j\Omega\hat{\mathbf{H}} = -j\mathbf{K}\times\hat{\mathbf{E}} = -\mathbf{a}_x jK_y\hat{E}_z + \mathbf{a}_y jK_x\hat{E}_z \tag{52}$$

so that the magnetic field components are given by

$$\hat{H}_x = \frac{K_y}{\mu\Omega}\hat{E}_z \tag{53}$$

$$\hat{H}_y = -\frac{K_x}{\mu\Omega}\hat{E}_z. \tag{54}$$

As before, $K_x$ has equal amplitude but opposite sign for the incoming and reflected waves.

Matching the $z$ component of the electric field at the interface dictates that the sum of the incoming and reflected fields must equal the transmitted field at $x = 0$. Since the phase must be equal along the boundary this reduces to

$$1 + \hat{\tilde{\Gamma}}_{tm} = \hat{\tilde{T}}_{tm}. \tag{55}$$

The other equation relating the reflection and transmission coefficients is obtained from Ampere's law applied to the nodes on the interface. Using (53) in (51) and rearranging yields

$$j\left(\Omega\epsilon_a - \frac{K_y^2}{\Omega\mu_a}\right)\hat{E}_z\Big|_{x=0} = \tilde{\partial}_x\hat{H}_y|_{x=0} \tag{56}$$

$$= \frac{1}{\delta}\left(\hat{H}_y^t\Big|_{x=\delta/2} - \hat{H}_{1y}|_{x=-\delta/2}\right) \tag{57}$$

where $\hat{H}_{1y}$ is the $y$ component of the sum of the incoming and reflected waves and $\hat{H}_y^t$ is the $y$ component of the transmitted field. After using (54) to express $\hat{H}_y$ in terms of $\hat{E}_z$ and discarding common phase terms, (57) yields

$$j\delta\left(\Omega^2\mu_a\epsilon_a - K_y^2\right)\hat{\tilde{T}}_{tm} = -\frac{\mu_a}{\mu_2}K_{2x}\hat{\tilde{T}}_{tm}e^{-j\kappa_{2x}} + \frac{\mu_a}{\mu_1}K_{2x}(e^{j\kappa_{1x}} - \hat{\tilde{\Gamma}}_{tm}e^{-j\kappa_{1x}}) \tag{58}$$

where the $\kappa$'s are defined in (37) and (38).

Using (55) and (58) to solve for the reflection coefficient yields

$$\hat{\tilde{\Gamma}}_{tm} = \frac{\frac{\mu_a}{\mu_1} K_{1x} e^{j\kappa_{1x}} - \frac{\mu_a}{\mu_2} K_{2x} e^{-j\kappa_{2x}} - j\delta\left(\Omega^2 \mu_a \epsilon_a - K_y^2\right)}{\frac{\mu_a}{\mu_1} K_{1x} e^{-j\kappa_{1x}} + \frac{\mu_a}{\mu_2} K_{2x} e^{-j\kappa_{2x}} + j\delta\left(\Omega^2 \mu_a \epsilon_a - K_y^2\right)}. \tag{59}$$

This can be compared to (45) of [4] which appears to have a typographical error. (The exponent of the first term in the numerator has the wrong sign. Also the term $K_z$ [with no numeric subscript] which appears in that expression is never explicitly defined.) The transmission coefficient is

$$\hat{\tilde{T}}_{tm} = \frac{2\frac{\mu_a}{\mu_1} K_{1x} \cos(\kappa_{1x})}{\frac{\mu_a}{\mu_1} K_{1x} e^{-j\kappa_{1x}} + \frac{\mu_a}{\mu_2} K_{2x} e^{-j\kappa_{2x}} + j\delta\left(\Omega^2 \mu_a \epsilon_a - K_y^2\right)}. \tag{60}$$

When, as was used in the $\mathrm{TE}^z$ case, $\epsilon_a$ is the average of the permittivity to either side of the interface, one can write

$$\delta\left(\Omega^2 \mu_a \epsilon_a - K_y^2\right) = \frac{\delta}{2}\left(\Omega^2 \mu_a \epsilon_1 + \Omega^2 \mu_a \epsilon_2 - 2K_y^2\right) \tag{61}$$

Assuming the permeability $\mu_a$ is the harmonic mean of the permeabilities to either side of the interface, i.e. $\mu_a = 2\mu_1\mu_2/(\mu_1 + \mu_2)$, the right-hand side of (61) can be written

$$\frac{\delta}{2}\left(\frac{2\mu_2}{\mu_1 + \mu_2}\left(\Omega^2 \mu_1 \epsilon_1 - K_y^2\right) + \frac{2\mu_1}{\mu_1 + \mu_2}\left(\Omega^2 \mu_2 \epsilon_2 - K_y^2\right)\right). \tag{62}$$

Using the dispersion relation (19), this becomes

$$\frac{\delta\mu_2}{\mu_1 + \mu_2} K_{1x}^2 + \frac{\delta\mu_1}{\mu_1 + \mu_2} K_{2x}^2. \tag{63}$$

Employing the definition of the $K$'s (17), allows us to write this imaginary term as

$$\frac{4\mu_2}{\delta(\mu_1 + \mu_2)} \sin^2(\kappa_{1x}) + \frac{4\mu_1}{\delta(\mu_1 + \mu_2)} \sin^2(\kappa_{2x}). \tag{64}$$

This final form is convenient because, assuming $\epsilon_a = (\epsilon_1 + \epsilon_2)/2$ and $\mu_a = 2\mu_1\mu_2/(\mu_1 + \mu_2)$, when the complex exponential in (59) and (60) are expanded it is clear that the imaginary part of that expansion identically cancels the term shown in (64). Thus, the resulting expressions are purely real and, after employing the double-angle formula, given by

$$\hat{\tilde{\Gamma}}_{tm} = \frac{\mu_2 \sin(2\kappa_{1x}) - \mu_1 \sin(2\kappa_{2x})}{\mu_2 \sin(2\kappa_{1x}) + \mu_1 \sin(2\kappa_{2x})} \tag{65}$$

$$\hat{\tilde{T}}_{tm} = \frac{2\mu_2 \sin(2\kappa_{1x})}{\mu_1 \sin(2\kappa_{1x}) + \mu_2 \sin(2\kappa_{2x})}. \tag{66}$$

These expressions reduce to that of the continuous world when the discretization goes to zero. Since the exact expressions are purely real, this serves as proof of the optimality of using the arithmetic mean for the interface permittivity and the harmonic mean for the permeability.

Implementation of an AFP TFSF boundary for the $\mathrm{TM}^z$ polarization also yields leaked fields which are approximately 100 dB down from the peak field when the incoming field is very coarsely discretized. Using a discretization which is typical of actual practice, the leaked field obtains a maximum of approximately $-180$ dB relative to the peak of the incoming field.

## VI. Conclusion

The AFP TFSF method can be readily applied to problems involving planar interfaces, whether dielectric or PEC. The method is ideally suited to oblique incidence and does not suffer the inherent approximations associated with using an auxiliary grid. If no wavenumber components are discarded from the transforms, the only errors associated with the technique would be those associated with implementation of the discrete-time Fourier transform. In practice, even when discarding superluminal wavenumber components and using a coarsely discretized incoming field, the leaked fields are approximately 100 dB down from the peak excitation. Using a discretization which is more typical of actual practice, the leaked fields are approximately 180 dB down. Modularized programs, written in C, which implement the AFP TFSF method for all the cases considered here are available from the authors.

The approach used here is not restricted to the second-order Yee FDTD algorithm. The same steps could be followed to derive an AFP TFSF technique for any FDTD method which has a rigorous dispersion relation. Additionally, the method could be applied to multiple layers where one would have to solve for the fields in the multi-layer system as is done in the continuous world.

## References


[1] D. E. Merewether, R. Fisher, and F. W. Smith, "On implementing a numeric Huygen's source scheme in a finite difference program to illuminate scattering bodies," *IEEE Trans. Nucl. Sci.*, vol. 27, no. 6, pp. 1829–1833, Dec. 1980.

[2] A. Taflove and S. Hagness, *Computational Electrodynamics: The Finite-Difference Time-Domain Method*, 3rd ed. Boston, MA: Artech House, 2005.

[3] C. Guiffaut and K. Mahdjoubi, "Perfect wideband plane wave injector for FDTD method," in *IEEE Antennas and Propagat. Soc. Int. Symp.*, Salt Lake City, UT, Jul. 2000, vol. 1, pp. 236–239.

[4] C. D. Moss, F. L. Teixeira, and J. A. Kong, "Analysis and compensation of numerical dispersion in the FDTD method for layered, anisotropic media," *IEEE Trans. Antennas. Propag.*, vol. 50, no. 9, pp. 1174–1184, Sep. 2002.

[5] J. B. Schneider, "Plane waves in FDTD simulations and a nearly perfect total-field/scattered-field boundary," *IEEE Trans. Antennas. Propag.*, vol. 52, no. 12, pp. 3280–3287, Dec. 2004.

[6] M. Celuch-Marcysiak and W. K. Gwarek, "On the nature of solutions produced by finite difference schemes in time domain," *Int. J. Numerical Modelling: Electronic Networks, Devices and Fields*, vol. 12, no. 1–2, pp. 23–40, Jan.–Apr. 1999.

[7] J. B. Schneider and R. J. Kruhlak, "Plane waves and planar boundaries in FDTD simulations," presented at the IEEE Antennas and Propagat. Soc. Int. Symp. and URSI Radio Sci. Meeting, Salt Lake City, UT, Jul. 2000.

[8] U. Oğguz and L. Gürel, "Interpolation techniques to improve the accuracy of the plane wave excitations in the finite difference time domain method," *Radio Sci.*, vol. 32, no. 6, pp. 2189–2199, Nov.–Dec. 1997.

[9] ——, "An efficient and accurate technique for the incident-wave excitations in the FDTD method," *IEEE Trans. Microw. Theory Tech.*, vol. 46, no. 6, pp. 869–882, Jun. 1998.

[10] S. C. Winton, P. Kosmas, and C. M. Rappaport, "FDTD simulation of TE and TM plane waves at nonzero incidence in arbitrary layered media," *IEEE Trans. Antennas. Propag.*, vol. 53, no. 5, pp. 1721–1728, May 2005.
[11] K. Demarest, R. Plumb, and Z. Huang, "FDTD modeling of scatterers in stratified media," *IEEE Trans. Antennas. Propag.*, vol. 43, no. 10, pp. 1164–1168, Oct. 1995.
[12] M. E. Watts and R. E. Díaz, "Perfect plane-wave injection into a finite FDTD domain through teleportation of fields," *Electromagn.*, vol. 23, no. 2, pp. 187–201, Feb.–Mar. 2003.
[13] R. E. Díaz and I. Scherbatko, "A simple stackable re-radiating boundary condition (rRBC) for FDTD," *IEEE Antennas Propag. Mag.*, vol. 46, no. 1, pp. 124–130, Feb. 2004.
[14] A. V. Oppenheim, A. S. Willsky, and I. T. Young, *Signals and Systems*. Englewood Cliffs, NJ: Prentice-Hall, 1983.
[15] J. B. Schneider and C. L. Wagner, "FDTD dispersion revisited: faster-than-light propagation," *IEEE Microw. Guided Wave Lett.*, vol. 9, no. 2, pp. 54–56, Feb. 1999.
[16] W. Ma, M. R. Rayner, and C. G. Parini, "Discrete Green's function formulation of the FDTD method and its application in antenna modeling," *IEEE Trans. Antennas. Propag.*, vol. 53, no. 1, pp. 339–346, Jan. 2005.
[17] L. N. Trefethen, "Group velocity in finite difference schemes," *SIAM Review*, vol. 24, no. 2, pp. 113–135, 1982.
[18] D. H. Choi and J. E. Roy, "The dispersion characteristics of the FD-TD method," in *Proc. IEEE Antennas and Propagat. Soc. Int. Symp.*, San Jose, CA, 1989, pp. 26–29.
[19] J. B. Schneider and R. J. Kruhlak, "Dispersion of homogeneous and inhomogeneous waves in the Yee finite-difference time-domain grid," *IEEE Trans. Microw. Theory Tech.*, vol. 49, no. 2, pp. 280–287, Feb. 2001.
[20] V. Anantha and A. Taflove, "Efficient modeling of infinite scatterers using a generalized total-field/scattered-field FDTD boundary partially embedded within PML," *IEEE Trans. Antennas. Propag.*, vol. 50, no. 10, pp. 1337–1349, Oct. 2002.
[21] J.-H. Chang and A. Taflove, "Three-dimensional diffraction by infinite conducting and dielectric wedges using a generalized total-field/scattered-field FDTD formulation," *IEEE Trans. Antennas. Propag.*, vol. 53, no. 4, pp. 1444–1454, Apr. 2005.
[22] F. D. Hastings, J. B. Schneider, and S. L. Broschat, "A Monte-Carlo FDTD technique for rough surface scattering," *IEEE Trans. Antennas. Propag.*, vol. 43, no. 11, pp. 1183–1191, Nov. 1995.
[23] E. I. Thorsos, "The validity of the Kirchhoff approximation for rough surface scattering using a Gaussian roughness spectrum," *J. Acoust. Soc. Amer.*, vol. 83, no. 1, pp. 78–92, 1988.
[24] Z. Wu and J. Fang, "High-performance PML algorithms," *IEEE Microw. Guided Wave Lett.*, vol. 6, no. 9, pp. 335–337, Sep. 1996.
[25] W. C. Chew and J. M. Jin, "Perfectly matched layers in the discretized space: An analysis and optimization," *Electromagn.*, vol. 16, no. 4, pp. 325–340, 1996.
[26] J. Fang and Z. Wu, "Closed-form expression of numerical reflection coefficient at PML interfaces and optimization of PML performance," *IEEE Microw. Guided Wave Lett.*, vol. 6, no. 9, pp. 332–334, Sep. 1996.
[27] J.-P. Bérenger, "Evanescent waves in PMLs: Origin of the numerical reflection in wave-structure interaction problems," *IEEE Trans. Antennas. Propag.*, vol. 47, no. 10, pp. 1497–1503, Oct. 1999.

**John B. Schneider** (M'00) received the B.S. degree in electrical engineering from Tulane University, New Orleans, LA, and the M.S. and Ph.D. degrees in electrical engineering from the University of Washington, Seattle.

He is presently an Associate Professor in the School of Electrical Engineering and Computer Science at Washington State University, Pullman. His research interests include the use of computational methods to analyze acoustic, elastic, and electromagnetic wave propagation.

**Kakhkhor Abdijalilov** received the M.S. degree in physics from Tashkent University, Uzbekistan and the Ph.D. degree in physics from the New Jersey Institute of Technology, Newark, NJ.

Currently he is a Research Associate with the School of Electrical Engineering and Computer Science of Washington State University, Pullman. His research interests include numerical methods for electromagnetics.